COBEM 2021 26th International Congress of Mechanical Engineering
November 22-26, 2021, Virtual Congress, Brazil

COB-2021-0449
STUDIES ON THE INFLUENCE OF CAVITATION BOUNDARY CONDITION MODEL ON THE PERFORMANCE OF TEXTURED SURFACE HYDRODYNAMIC JOURNAL BEARINGS

Luiz Fellipe Nogueirão
Flávio Yukio Watanabe
Federal University of São Carlos
Rod. Washington Luís, km 235 - São Carlos - SP - Brazil, CEP 13.565-905
nogueirao.luiz@gmail.com, fywatanabe@ufscar.br

Abstract. *Textured surfaces can be found in many situations where one search through its use a way of improving specific characteristics. An up-to-date literature review is made for identifying the static analysis methods for texturized hydrodynamic journal bearings. A comparison of the boundary condition types is elaborated for a cylindrical non texturized hydrodynamic journal bearing. The present study traces to evaluate the influence of textured surfaces through a model that is discretized by the finite difference method. The textures are considered as spherical grooves distributed on a specific pattern along the surface of the hydrodynamic cylindrical journal bearing. The study starts with an initial model considering the Gümbel boundary condition and comparing the results with a calculation that considers the Swift-Stieber boundary conditions. After validating the model, some cases for cylindrical journal bearings with large cavities are analyzed. The results show as expected losses on most of the cases for the load capacity. The next steps are to improve the model with one that respects the mass conservation with the JFO boundary condition and to analyze bearings with micro sized cavities.*

Keywords: *tribology, surface engineering, mass-conserving cavitation model, finite difference method, spherical grooves*

1. INTRODUCTION

Surface texturing is defined as the intentional insertion of identical details respecting a pattern on a surface. The application of a specific pattern is the main difference between texturing and roughness, where the last is randomly distributed on the surface (Gropper *et al.*, 2015).

The generation of this controlled pattern is a challenge that has shown major evolutions in the last decades, thanks to the emergence of manufacturing techniques in micrometric scale (Tala-Ighil *et al.*, 2007). Ibatan *et al*. (2015) mention options for generating textures such as: surface laser texturing, micro milling, micro casting and electrochemical machining.

With the overcoming of the microgeneration barriers of textures, tribological studies to analyze their effect emerged. Among the studies listed by Gropper *et al*. (2015) on the topic of surface texturing, 55% are theoretical and 26% experimental. Theoretical studies are carried out through the development of mathematical models that seek to simulate operating conditions under the influence of textures. Experimental studies are mostly performed on test benches for tribological analysis, such as pin-on-disc and ball-on-disc types.

The study by Tala-Ighil *et al*. (2007), one of the pioneers on the subject, analyzes the variation in bearing performance under the influence of textures. The performance is analyzed by the resulting modification of the oil film thickness (directly related to load capacity) and of the frictional torque (inversely related to efficiency). Wakuda *et al*. (2003) also mention other possible advantages of using textures, such as: texture serves as a local oil reservoir, aiding in lubrication in cases of momentary oil shortages; textures could serve as particulate capture points (debris). Tang *et al*. (2013) report practical experiments to analyze these possible advantages.

According to Ibatan *et al*. (2015) there is still great divergence in the conclusions of the influences of textures on the performance of hydrodynamic bearings. This due to the lack of consensus on what would be the best models and procedures for the analysis.

This study seeks to analyze the influence of texturing through a computational mathematical model. The model consists of discretizing the radial sliding bearing using the finite difference method to solve the modified Reynolds equation that considers the cavitation effects. To achieve this model, the evolution of the computational models used and the recommendations for textured journal bearings are analyzed.

2. MATHEMATICAL FORMULATION

Reynolds (1886) analyzes the experiments carried out by Beauchamp Tower in 1883 and 1884 to propose in his study the classical Reynolds equation, Eq. (1), that describes the formation of the pressure profile in hydrodynamic bearings.

$$\frac{\partial}{\partial x}\left(\rho h^3 \frac{\partial P}{\partial x}\right) + \frac{\partial}{\partial z}\left(\rho h^3 \frac{\partial P}{\partial z}\right) = 6\mu\left\{(U_0 + U_1)\frac{\partial \rho h}{\partial x} + 2V_1\right\} \tag{1}$$

where:

P - fluid film pressure
x, z - circumferential and axial coordinates, respectively
h - fluid film thickness
μ - oil film viscosity
ρ - oil film density
U_0, U_1 – circumferential component of the bearing and shaft's surface velocities, respectively
V_1 – radial component of the shaft's surface velocity

The Reynolds equation assumes that the gap is completely filled with oil and that the pressure is positive in regions where the gap decreases and negative in regions where the gap increases. However, in practice, while positive pressures do not have an upper limit, negative pressures do. When reaching this limit value for negative pressures, there is the phenomenon of oil rupture, and the pressure cannot decrease any further. The oil rupture phenomenon is complex because it involves several factors, for example, cavitation and even the fact that this region reaches lower pressure values than the environment, thus allowing the entry of air or external fluids (Hori, 2006).

The options of boundary conditions to be applied in the oil film rupture region evolved on the last decades. The selection of which condition to use depends on the nature of the problem.

2.1 Circumferential boundary conditions without mass conservation

The solution of the Reynolds equation by Sommerfeld (1914) does not consider the rupture of the oil film, allowing the pressure distribution to reach sub-atmospheric and even negative values (Figure 1a). In a way to approximate the results of practical experiments, Gümbel (1914) presents a boundary condition that turns all negative pressure values to zeros (Figure 1b). This boundary condition is also called half-Sommerfeld.

The Gümbel boundary condition violates the continuous flow principle by abruptly resetting the negative values of the pressure field (Khonsari and Booser, 2008). Khonsari and Booser (2008) state that Reynolds (1886) was aware of the problems associated with the boundary condition in the divergent region of the oil film, but it is Swift (1932) and Stieber (1933) who independently present a new boundary condition that considers that the rupture region of the oil film occurs gradually, obeying the condition that $\partial P/\partial x = 0$ (Figure 1c). This boundary condition is also called the Reynolds boundary condition.

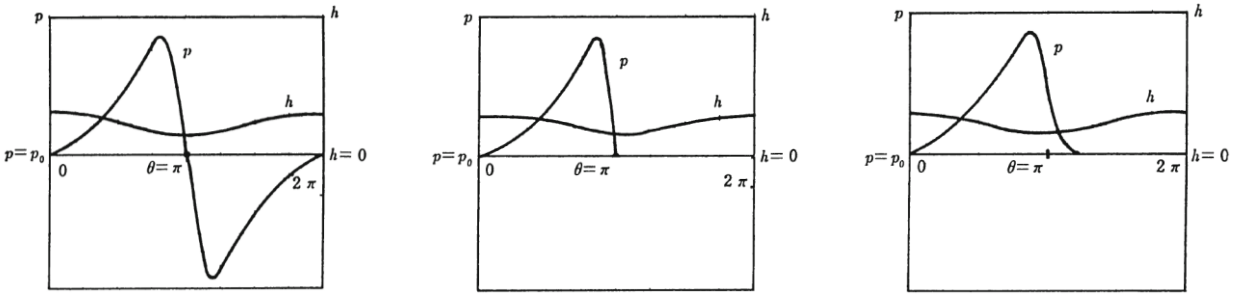

(a) Sommerfel (b) Gümbel (Half-Sommerfeld) (c) Swift-Stieber (Reynolds)

Figure 1 Circumferential pressure boundary conditions for journal bearings (Someya, 1989).

As discussed, the convergence of the oil film leads to an increase in pressure and after it exceeds the region of maximum pressure, the oil film increases its thickness again. The pressurized oil cannot occupy this increased gap, thus generating the rupture of the oil film that usually occurs in finger-shaped voids (Khonsari and Booser, 2008), as illustrated in Figure 2. This phenomenon is considered in the Swift-Stieber condition and receives the term gaseous cavitation, but it is the Jakobsson-Flober-Olsson (JFO) theory that is more advanced to describe it (Braun and Hannon, 2010).

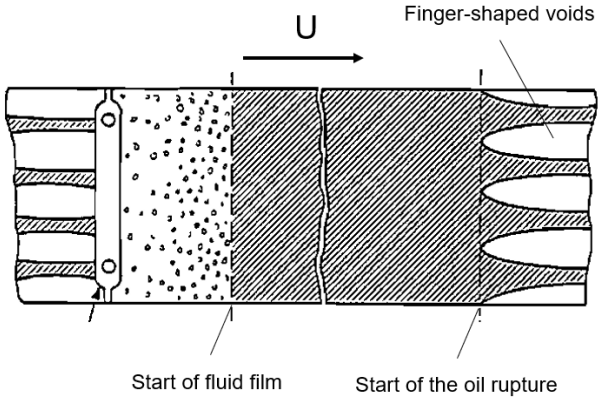

Figure 2: Oil rupture region (Heshmat, 2008).

Ausas *et al.* (2007) report that the application of a model without mass conservation, while analyzing textured bearings, overestimates the gain in carrying capacity. The study recommends the use of models with conservation of mass, such as models that follow the JFO theory.

2.2 Circumferential boundary conditions with mass conservation

Jakobsson and Floberg (1957) and Olsson (1965) present a theory of cavitation that guarantees an adequate compromise between practicality and precision. The theory is identified as JFO and divides the oil film into two regions: the first region with complete film formation obeys the classic Reynolds equation (Eq. 1); the second region starts with the rupture of the oil film. In this second region, only part of the gap is filled with oil and the pressure is considered constant, thus, the terms of the classic Reynolds equation, Eq. (1), dependent to pressure are zeroed out (Elrod, 1981).

The JFO boundary condition results from the application of mass conservation in the full-film interface and cavitation zones (Elrod, 1981). JFO theory received several algorithms for its implementation (Braun and Hannon, 2010).

2.3 Modified Reynolds Equation

Elrod and Adams (1974) present a modified Reynolds equation that describes the hydrodynamic conditions in the full-film and cavitation regions according to the JFO theory. The Elrod and Adams (1974) algorithm is improved and presented by Elrod (1981), and three new variables are presented, θ, β_ρ and g, and these are inserted in the classical Reynolds equation.

$$\theta = \frac{\rho}{\rho_{cav}} \tag{2}$$

where:

ρ - oil film density

ρ_{cav} - density of the oil film in the cavitation region where the pressure is constant and equals P_{cav}

θ is a dimensionless value that indicates whether the location is in the cavitation region or not:

- If $\theta < 1$, the local density is lower than the density ρ_{cav}, therefore, there is a rupture condition due to the cavitation region.
- If $\theta \geq 1$, there is complete formation of the oil film.

The second variable required, Eq. (3), is the constant β_ρ, bulk modulus or compressibility factor which determines the relationship between density and pressure (Braun and Hannon, 2010):

$$\beta_\rho = \rho \frac{\partial P}{\partial \rho} \tag{3}$$

And the third variable, Eq. (4) needed is the g shift function:

$$g = g(\theta) \tag{4}$$

- If $\theta < 1 \rightarrow g=0$, that is, there is the condition of cavitation.
- If $\theta \geq 1 \rightarrow g=1$, that is, there is the complete formation of the oil film.

By differentiating Eq. (2) and replacing it in Eq. (3):

$$\beta_\rho = \theta \frac{\partial P}{\partial \theta} \tag{5}$$

Vijayaraghavan and Keith Jr. (1988) apply an improvement to Elrod's (1981) algorithm by combining the switch function g to expression (5):

$$\partial P = \frac{g(\theta)\beta_\rho}{\theta} \partial \theta \tag{6}$$

Equation (2) and (6) are replaced in the classical Reynolds equation, Eq. (1) and the bearing surface is considered static ($U_0 = V_1 = 0$):

$$\frac{\partial}{\partial x}\left(\beta_\rho h^3 g(\theta) \frac{\partial \theta}{\partial x}\right) + \frac{\partial}{\partial z}\left(\beta_\rho h^3 g(\theta) \frac{\partial \theta}{\partial z}\right) = 6\mu U_1 \frac{\partial \theta h}{\partial x} \tag{7}$$

Equation (7) is the modified Reynolds equation of Elrod (1981) with modifications by Vijayaraghavan and Keith Jr. (1988).

The solution of the modified Eq. (7) gives the distribution of the density ratio θ, which includes the distribution of regions of complete oil film formation and regions with cavitation. Having the distribution of θ along the bearing, it is possible to obtain the pressure distribution P through the integration of Eq. (6), which results in:

$$P = g(\theta)\beta_\rho \ln \theta + P_{cav} \tag{8}$$

It is thus possible, through Eq. (8), to obtain the pressure distribution P in a hydrodynamic radial bearing, including the cavitation effects.

2.4 Modeling with surface textures

The classical Reynolds equation, Eq. (1), and the modified Reynolds equation, Eq. (7), make it possible to analyze several types of bearings, for example, cylindrical, lemon and off-set bearings. For this, it is necessary to establish the expression of the oil film profile $h(\alpha)$ for each type of bearing, where α is a circumferential angular coordinate. For cylindrical bearings, the oil film profile $h(\alpha)$ is expressed as a function of the clearance c, the eccentricity e and the attitude angle β:

$$h(\alpha) = c + e\cos(\alpha - \beta) \tag{9}$$

The addition of bearing textures can be interpreted as adding extra heights to the oil film, so the final oil film profile is stated as:

$$h_f(\alpha, z) = h(\alpha) + h'(\alpha, z) \tag{10}$$

Where, $h'(\alpha, z)$ describes the distribution of textures along the bearing. This distribution indicates the number, position, and shape of textures. For this study, the textures were considered as cavities with a sinusoidal shape:

$$\begin{cases} h'(\alpha,z) = r_y \cdot \sin\left(\dfrac{r-(x_c-x)}{r}\right) \cdot \sin\left(\dfrac{r-(z_c-z)}{r}\right) & \text{, if } \sqrt{(x-x_c)^2+(z-z_c)^2} \le r \\ h'(\alpha,z) = 0 & \text{, otherwise} \end{cases} \tag{11}$$

where:

r_y - maximum depth of the texture

r - radius of the texture on the bearing surface

x_c and z_c - coordinates for positioning each texture

3. NUMERICAL SOLUTION

The solution for finite bearings using the classical Reynolds equation, Eq. (1), or the modified equation, Eq. (7), is only possible with a numerical method.

This study is carried out using the finite difference method (FDM) due to its greater ease of implementation and greater number of references.

According to Gropper (2006), special attention should be paid to discretization when using FDM. For the modified Reynolds Eq. (7), a specific type of differentiation must be used for the region of complete formation of the oil film ($g = 1$) and for the region of cavitation ($g = 0$):

- The region of complete formation of the oil film ($g = 1$) is equivalent to the condition described by the classical Reynolds Eq. (1), which is an elliptic partial differential equation. For this type of equation, centered numerical differentiation is appropriate (Vijayaraghavan and Keith Jr., 1988).
- The cavitation region ($g = 0$) generates a hyperbolic partial differential equation. For this type of equation, progressive numerical differentiation (upwind) is appropriate (Vijayaraghavan and Keith Jr., 1988).

Vijayaraghavan e Keith (1988) present a method to automate these two types of differentiation by adding an artificial viscosity term to the modified Reynolds equation. The convergence of the problem may be obtained through several methods, having been chosen for this study the method of Gauss Seidel with successive over relaxation.

All the models are isothermal, that is, the temperature is constant and so the viscosity. To bring the simulations closer to a real situation, a simple thermal balance is performed using DIN 31652 to obtain an average temperature for the oil film and so correcting the operating viscosity.

4. STATIC CHARACTERISTICS OF RADIAL BEARINGS

With the pressure distribution, it is possible to obtain parameters to analyze the performance of the bearing in operation. The load capacity W of a bearing is obtained by the numerical integration of the pressure profile in the directions of the eccentricity W_x and perpendicular to it W_y:

$$\begin{cases} W_x = \int_0^L \int_0^{2\pi} PR\cos\alpha \, d\alpha \, dz \\ W_y = \int_0^L \int_0^{2\pi} PR\sin\alpha \, d\alpha \, dz \end{cases} \quad \Rightarrow W = \sqrt{W_x^2 + W_y^2} \tag{12}$$

Where, L and R are the bearing's length and radius, respectively.

The load capacity W has the same intensity as the force F applied to the shaft, but both have opposite directions.

With it load capacities on both directions it is possible to calculate the attitude angle β:

$$\tan\beta = \frac{W_y}{W_x} \tag{13}$$

For performance analysis, the greater the load capacity W, the greater is the hydrodynamic support of the generated oil film.

A second parameter for analyzing the bearing performance is the viscous dissipation generated in operation. Viscous dissipation in radial bearings is composed by the fluid shear stresses on the surfaces of the bearing and rotor (Hori, 2006). This term is also known as friction torque, M_r, and may be calculated by Eq. (14).

$$M_r = \int_o^L \int_0^{2\pi} \left(\frac{\mu U}{h} + \frac{h}{2R} \frac{dP}{d\alpha} \right) R^2 L \, d\alpha dz \tag{14}$$

The smaller the friction torque M_r, the smaller is the viscous dissipation, and thus, the greater is the bearing efficiency in terms of power savings.

5. NUMERICAL SIMULATIONS

First, a computational routine is elaborated in GNU Octave (2019) to solve the classical Reynolds equation with the FDM for a bearing without textures. For this first model, the Gümbel boundary condition is used, without breakage of the oil film and without mass conservation, for future comparison with other boundary conditions. This elaborated routine is isothermal but receives the adjusted viscosity values for the average oil film temperature according to DIN 31652.

The solution by the classic Reynolds Eq. (1) and Gümbel boundary condition of the bearing without textures is compared with a solution using DIN 31652. DIN 31652 also uses the classical Reynolds equation but considers the Swift-Stieber (Reynolds) boundary condition, that is, with rupture of the oil film, but without mass conservation.

5.1 Results without textures

Table 1 shows the considered input data for the bearing analysis.

Table 1. Bearing input data for the analysis.

Parameters and units	Value
Geometric characteristics of the analysis	
Diameter [mm]	225,00
Width [mm]	170,00
Radial clearance *c* [mm]	0,166
Operational characteristics of the analysis	
Shaft rotational speed [rpm]	1800,00
Eccentricity due to load *e*[mm]	0,125
Lubricating fluid characteristics of the analysis	
Oil type	ISO VG 68
Density [kg/m³]	870,00
Oil input temperature [°C]	45,0
Oil mean temperature according to DIN 31652 [°C]	60,0
Oil mean viscosity adjusted to its mean temperature [mPas]	24,28

The routine developed in GNU Octave (2019) uses the bearing discretized by 709 nodes in the circumferential direction (α) and 87 nodes in the width (z). It is noteworthy that the routine solves the problem for half the bearing's width, considering that its construction and future texture positions are symmetric.

Table 2 shows the obtained results:

Table 2. Results obtained for plain bearing.

Results and units	GNU Octave	DIN 31652
Load capacity W [kN]	141,79	155,00
Attitude angle β [°]	44,12	36,94
Minimum film thickness h_0 [mm]	0,041	0,041
Maximum oil pressure [MPa]	11,90	NA
Circumferential position of the maximum oil pressure [°]	198,31	NA

The load capacity W obtained in GNU Octave (2019) is about 9% lower than that obtained in DIN 31652. This is probably related to the Gümbel boundary condition applied in GNU Octave (2019) which disregards any cavitation effect in the divergent region of the oil film, whereas DIN 31652 considers the extra support in the film rupture region thanks to the Swift-Stieber (Reynolds) condition.

DIN 31652 does not generate pressure distribution curves, so there is no information regarding the maximum pressure and its angular position. The pressure curve obtained in the routine in GNU Octave (2019) follows in the Figure 3. The Gümbel condition abruptly resets the pressure distribution in the divergent region of the oil film.

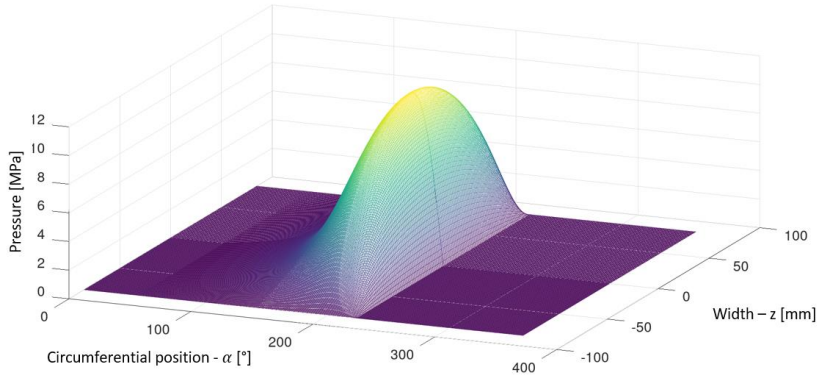

Figure 3. View of the divergent region of the pressure distribution obtained by GNU Octave (2019).

5.2 Bearing results with textures

After performing the tests for plain bearings (without textures), simulations with large scale textures are started. See the dimensions of the textures considered in the Table 3.

Table 3. Cavity geometries considered in the analysis.

Parameters and units	**Value**
Maximum texture depth r_y [microns]	300
Texture radius on the surface r [microns]	8000

The analyzed cases follow in the Table 4. Initially, only cases 1 to 4 where analyzed. Case 5 is explained later.

Table 4. Position of the cavities for each case analyzed.

Case	**Number of cavities**	**Circumferential position α_c [°]**	**Width position z_c [mm]**
1	1	180	0
2	3	180; 180; 180	+L/4; 0; -L/4
3	3	90; 180; 270	0; 0; 0
4	6	90; 180; 270; 90; 180; 270	+L/3; +L/3; +L/3; -L/3; -L/3; -L/3
5	2	90; 270	0; 0

The Figure 4 below shows the oil film profiles obtained for the cases analyzed in the Table 4.

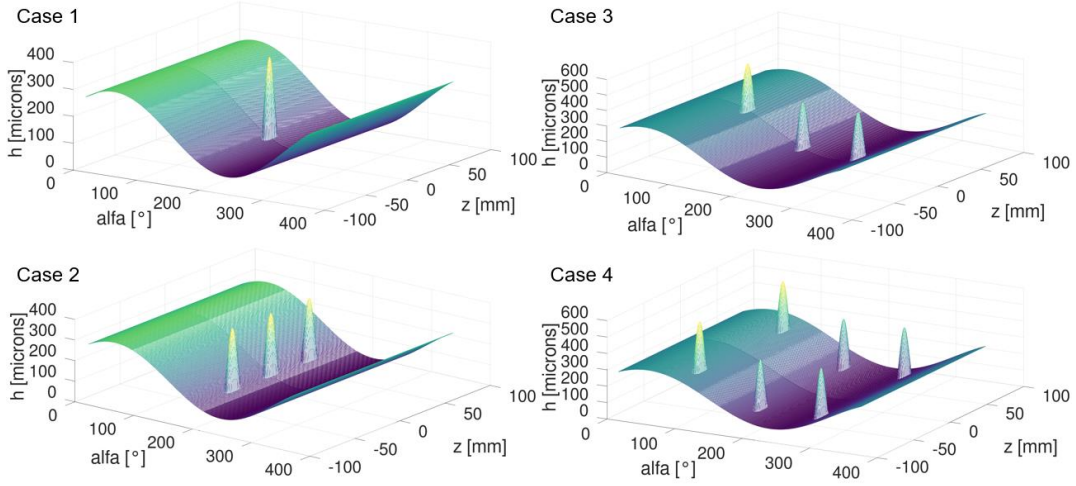

Figure 4. Oil film profiles for cases 1, 2, 3 and 4.

In the **Erro! Fonte de referência não encontrada.** 5 and Figure 6, the pressure distributions obtained are shown and the numerical results are summarized in the Table 5.

Table 5. Comparison between plain bearing results and cases 1 to 4 with cavities.

Results and units	**No cavities**	**Case 1**	**Case 2**	**Case 3**	**Case 4**
Load capacity W [kN]	141,79	140,70	136,70	140,79	138,37
Attitude angle β [°]	44,12	44,30	44,63	44,17	44,17
Maximum pressure [MPa]	11,90	11,70	11,40	11,71	11,71
Circumferential position of the maximum pressure [°]	198,31	199,32	199,31	198,81	198,81

As expected, the large cavities reduce the load capacity. Cases 2 and 4, which have a greater number of cavities in the region of highest pressure, were the cases that had the greatest reduction, reaching 3%.

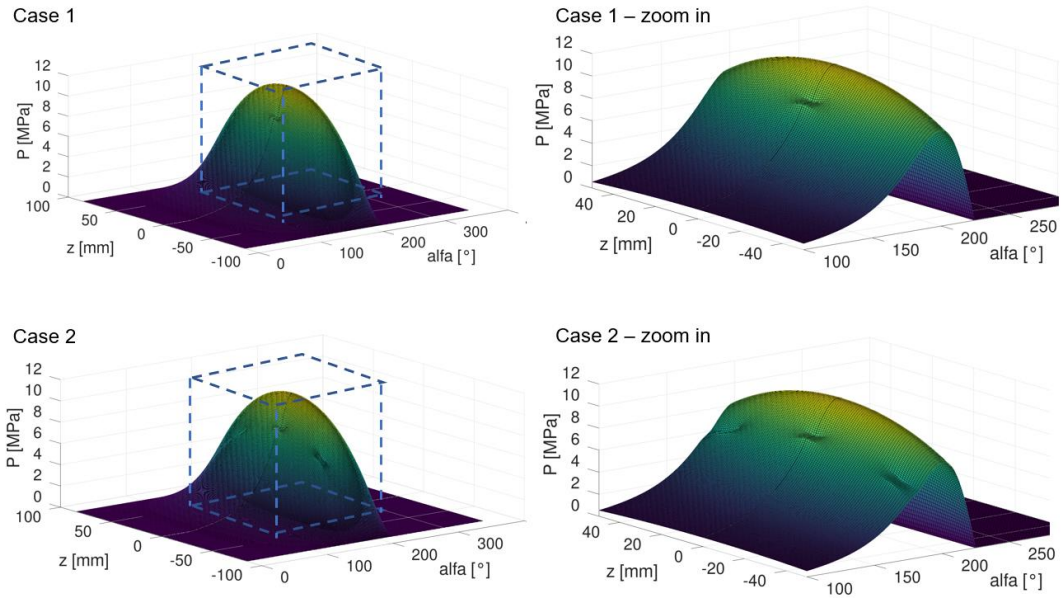

Figure 5. Pressure profiles for cases 1 and 2 with their respective zoom view for analysis of the textures influence.

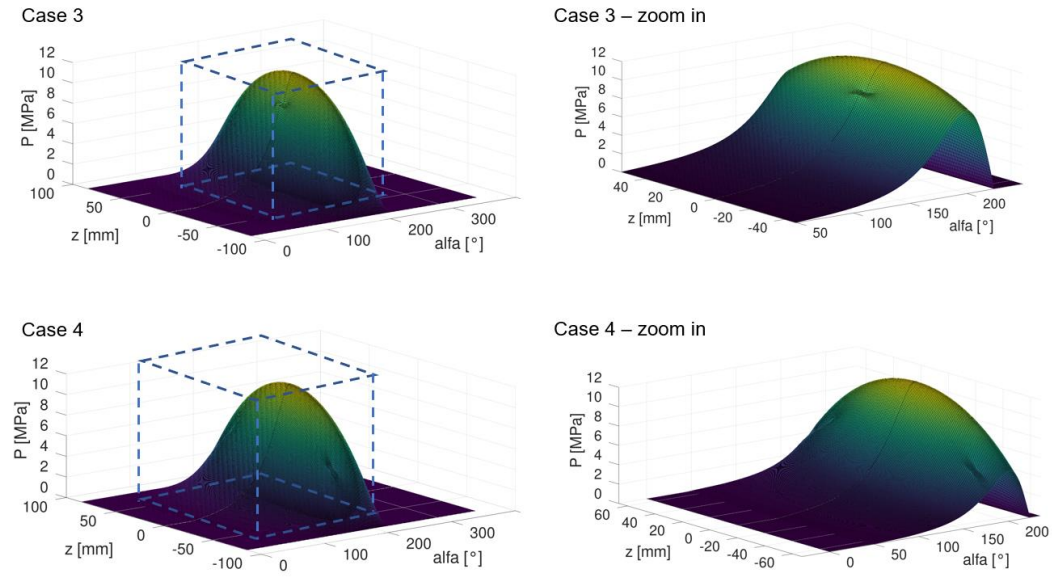

Figure 6. Pressure profiles for cases 3 and 4 with their respective zoom view for analysis of the textures influence.

Case 3, even though having two more cavities than case 1, showed the smallest reductions in load capacity. This result prompted a further analysis, removing the cavity in the center of case 3. Table 4 shows data for case 5, the fifth analysis texture settings.

Figure 7a shows the oil film profiles obtained for the case 5 and Figure 7b the corresponding pressure distribution. In Table 6, the results of cases, 1, 3 and 5 are compared.

Table 6. Comparison between the results of plain bearing and cases 1, 3 and 5 with cavities

Results and units	**No cavities**	**Case 1**	**Case 3**	**Case 5**
Load capacity W [kN]	141,79	140,70	140,79	141,87
Attitude angle β [°]	44,12	44,30	44,17	43,98
Maximum pressure [MPa]	11,90	11,70	11,71	11,92
Circumferential position of the maximum pressure [°]	198,31	199,32	198,81	198,30

Figure 7. Oil film and pressure profiles for case 5

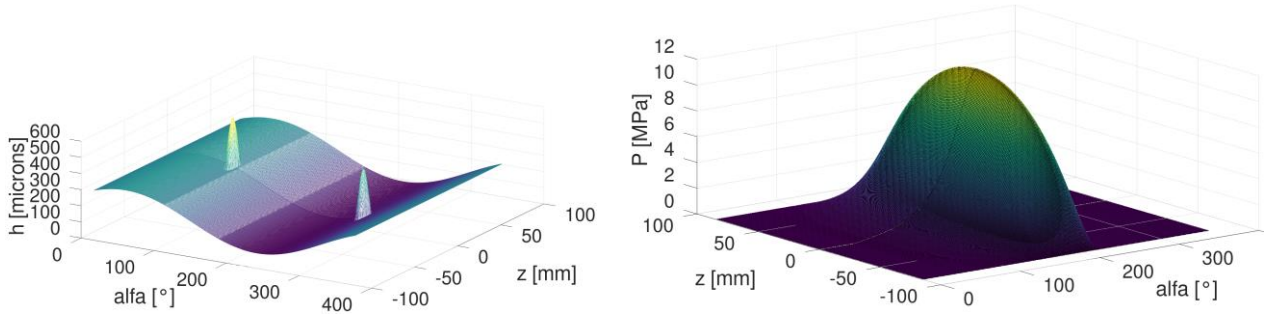

(a) Oil film profile (b) Pressure profile

For case 5, no effects of the texture are graphically noted. Still, according to Table 6, the textures result on a pressure configuration different from the other previous cases. The load capacity of case 5 is even higher than the load capacity of the case without cavities. This justifies the load gain from case 3 to case 1 and is in line with conclusions from other studies that indicate that the distribution of cavities in appropriate locations can be beneficial to the bearing (Ramos, 2018; Tala-Ighil *et al.*, 2011; Tang *et al.*, 2013; Lin *et al.*, 2015 and Ibatan *et al.*, 2015).

6. CONCLUSIONS AND FUTURE PERSPECTIVES

The model developed, even with simpler boundary conditions that do not consider the cavitation phenomenon, exhibits consistent results by providing lower load capacities than the results obtained from the DIN 31652 that considers film rupture, and so, an extra load capacity at its region. This conclusion about the difference in values is supported by the literature review. The same review was important to determine the next steps of the study.

The analysis with macro cavities were important for the transition to a more complex model. The results with the cavities met the expected by showing the loss of load capacity. However, the load capacity gain results of case 5 were surprising. Even with reports in the literature of gains in carrying capacity with texturing, it was not expected to obtain a gain in the initial analyses, especially with macro cavities. This specific case should be re-evaluated at the end of the study, where it is hoped to have a more complete model that contains the cavitation effects.

7. REFERENCES

Ausas, R., Ragot, P., Leiva, J., Jai, M., Bayada, G., Buscaglia, G. C., 2007. "The Impact of the Cavitation Model in the Analysis of Microtextured Lubricated Journal Bearings". *Transactions of the ASME*, Vol. 129, pp. 868-875.

Braun, M. J., Hannon, W. M., 2010. "Cavitation formation and modelling for fluid film bearings: a review". *Journal of Engineering Tribology*, Vol. 224, No. 9, pp. 839-863.

DIN, 1983, *Deutsches Institut für Normung e. V., - DIN 31652 - Teil 1. Hydrodynamische Radial-Gleitlager im stationären Betrieb*. *Berechnung von Kreiszylinderlagern*. Berlin: Beuth Verlag GmbH.

Elrod, H. G., Adams, M. L., 1974. "A computer program for cavitation and starvation problems". *Proceedings of the first Leeds-Lyon Symposium on Tribology*. Leeds.

Elrod, H. G., 1981. "A Cavitation Algorithm". *Journal of Lubrication Technology*, Vol. 103, No. 3, pp. 350-354.

GNU Octave v. 5.1.0, 2019. John W. Eaton and others.

Gropper, D., Wang, L., Harvey, T. J., 2016. "Hydrodynamic lubrication of textured surfaces: A review of modeling techniques and key findings". *Tribology International*, Vol. 94, pp. 509-529.

Gümbel, L., 1914. "Das Problem der Lagerreibung". *Berlin Bezirksverein*, Vol. 5, pp. 87-104 and pp. 109-120.

Heshmat, H, 1991. "The Mechanism of Cavitation in Hydrodynamic Lubrication". *Tribology Transactions*, Vol. 32, No. 2, pp. 177-186.

Hori, Y., 2006. *Hydrodynamic Lubrication*. Tokyo Springer Verlag.

Ibatan, T., Uddin, M. S., Chowdhury, M. A. K., 2015. "Recent development on surface texturing in enhancing tribological performance of bearing sliders". *Surface & Coatings Technology*, Vol. 272, pp. 102-120.

Jakobbson, B., Floberg, L., 1957. "The finite journal bearing, considering vaporization". *Transactions of Chalmers University Technology*, Goteborg, Sweden, Vol. 190, pp. 1-119.

Khonsari, M. M., Booser, E. R., 2008. *Applied Tribology: Bearing Design and Lubrication*. 2nd ed. Chichester: John Wiley & Sons, Ltd.

Lin, Q., Wei, Z., Wang, N., Chen, W., 2015. "Effect of large-area texture/slip surface on journal bearing considering cavitation". *Industrial Lubrication and Tribology*, Vol. 67, No. 3, pp. 213-226.

Olsson, K., 1965. "Cavitation in dynamically loaded bearings". *Transactions of Chalmers University Technology*, Goteborg, Sweden, Vol. 308.

Ramos, L. T., 2018. *Modelagem de Mancais Hidrodinâmicos com Efeitos de Texturização Superficial*. Doctoral Dissertation - Graduate Program in Mechanical Engineering, University of Campinas, Campinas.

Reynolds, O., 1886. "On the theory of lubrication and its application to Mr. Beauchamp Tower's experiments, including an experimental determination of the viscosity of olive oil". *Philosophical Transactions of the Royal Society of London*, Vol. 177, pp. 157-234.

Someya, T., 1989. *Journal-Bearing Databook*. Berlin-Heidelberg: Springer-Verlag.

Sommerfeld, A., 1904. "Zur hydrodynamische Theorie der Schmiermittelreibung". *Zeit Math. Phys*. Vol. 50, pp. 97-155.

Stieber, W., 1933. "Das schwimmlager: Hydrodynamische Theorie des Gleitlagers". *VDI Verlag*, GmbH, Berlin.

Swift, H. W., 1932. "The stability of lubricating films in journal bearings". *Proceedings of the institution of civil engineers*. Vol. 233, pp. 267-288.

Tala-Ighil, N. Maspeyrot, P., Fillon, M., Bounif, A., 2007. "Effects of surface texture on journal-bearing characteristics under steady-state operating conditions". *Journal of Engineering Tribology*, Vol. 221, No. 6, pp. 623-633.

Tala-Ighil, N., Fillon, M., Maspeyrot, P., 2011. "Effect of textured area on the performances of a hydrodynamic journal bearing". *Tribology International*, Vol. 44, pp. 211-219.

Tang, W, Zhou, Y, Zhu, H., Yang, H., 2013. "The effect of surface texturing on reducing the friction and wear of steel under lubricated contact". *Applied Surface Science*, Vol. 273, pp. 199-204.

Vijayaraghavan, D., Keith JR. T. G., 1988. "Development and Evaluation of a Cavitation Algorithm". *Tribology Transactions*. Vol. 32, pp. 225-233.

Wakuda, M., Yamauchi, Y., Kanzaki, S., Yasuda, Y., 2003. "Effect of surface texturing on friction reduction between ceramic and steel materials under lubricated sliding contact". *Wear*. Vol. 254, pp. 356-363.

8. RESPONSIBILITY NOTICE

The authors are the only responsible for the printed material included in this paper.